*Molecular Vision* 2016; 22:1077-1094 <http://www.molvis.org/molvis/v22/1077>
Received 20 May 2016 | Accepted 7 September 2016 | Published 9 September 2016



# Three-dimensional retinal organoids from mouse pluripotent stem cells mimic *in vivo* development with enhanced stratification and rod photoreceptor differentiation

**Holly Yu Chen,[1] Koray Dogan Kaya,[1] Lijin Dong,[2] Anand Swaroop[1]**

*[1]Neurobiology-Neurodegeneration and Repair Laboratory, National Eye Institute, National Institutes of Health, Bethesda, MD; [2]Genetic Engineering Core, National Eye Institute, National Institutes of Health, Bethesda, MD*

**Purpose:** The generation of three-dimensional (3D) organoids with optic cup–like structures from pluripotent stem cells has created opportunities for investigating mammalian retinal development *in vitro*. However, retinal organoids in culture do not completely reflect the developmental state and *in vivo* architecture of the rod-dominant mouse retina. The goals of this study were to develop an efficient protocol for generating retinal organoids from stem cells and examine the morphogenesis of rods *in vitro*.

**Methods:** To assess rod photoreceptor differentiation in retinal organoids, we took advantage of *Nrl*-green fluorescent protein (GFP) mice that show rod-specific expression of GFP directed by the promoter of leucine zipper transcription factor NRL. Using embryonic and induced pluripotent stem cells (ESCs and iPSCs, respectively) derived from the *Nrl*-GFP mouse, we were successful in establishing long-term retinal organoid cultures using modified culture conditions (called High Efficiency Hypoxia Induced Generation of Photoreceptors in Retinal Organoids, or HIPRO).

**Results:** We demonstrated efficient differentiation of pluripotent stem cells to retinal structures. More than 70% of embryoid bodies formed optic vesicles at day (D) 7, >50% produced optic cups by D10, and most of them survived until at least D35. The HIPRO organoids included distinct inner retina neurons in a somewhat stratified architecture and mature Müller glia spanning the entire retina. Almost 70% of the cells in the retinal organoids were rod photoreceptors that exhibited elongated cilia. Transcriptome profiles of GFP+ rod photoreceptors, purified from organoids at D25–35, demonstrated a high correlation with the gene profiles of purified rods from the mouse retina at P2 to P6, indicating their early state of differentiation.

**Conclusions:** The 3D retinal organoids, generated by HIPRO method, closely mimic *in vivo* retinogenesis and provide an efficient *in vitro* model to investigate photoreceptor development and modeling disease pathology.

Rod and cone photoreceptors are specialized retinal neurons that initiate the visual process. While cone photoreceptors mediate color and daylight vision, rod photoreceptors function in dim light and can capture even a single photon [1]. Dysfunction of photoreceptors is the primary cause of vision impairment in most retinal and macular degenerative diseases [2]. Genetic and genomic studies have uncovered almost 250 genes for inherited retinal diseases (RetNet), and at least 52 common and rare variants at 34 distinct genetic loci have been associated with age-related macular degeneration [3,4]. At this stage, few treatment options are available. Gene therapy appears to have some initial success in treating visual dysfunction caused by specific inherited genetic mutations [5-8]. However, extensive genetic and phenotypic heterogeneity observed in retinal and macular degeneration strongly argues for the development of additional therapeutic strategies. Network- or pathway-based design of drugs and optogenetics have demonstrated promise in preclinical studies [9,10], and the feasibility of photoreceptor cell replacement has been demonstrated for repairing degenerated retinas in mice [11,12]. Transplanted retinal progenitors or rod photoreceptors from embryonic pluripotent stem cells (ESCs) or induced pluripotent stem cells (iPSCs) have been shown to integrate into the mouse retina, express photoreceptor-specific proteins, and partially restore some vision of recipient mice [13-17]. These proof-of-principle studies strongly suggest that transplantation of ESCs or iPSC-derived photoreceptors can be used as a promising approach for the treatment of retinal degeneration diseases.

With the advent of a three-dimensional (3D) culture system, retinal organoids can be generated from pluripotent stem cells using serum-free floating cultures of embryoid body-like aggregates with quick reaggregation (SFEBq) methodology [18,19]. The 3D retinal organoids seem to mimic the dynamic processes of retinal morphogenesis *in vivo*, including evagination of neuroepithelia to form optic vesicles and subsequent invagination to produce optic cups.

Correspondence to: Anand Swaroop, Neurobiology-Neurodegeneration and Repair Laboratory, National Eye Institute, National Institutes of Health, Bethesda, MD 20892; Phone: (301) 435 5754; FAX: (301) 480 9917; email: swaroopa@nei.nih.gov

The neural retina in 3D cultures appears to be structurally similar to the mammalian retina *in vivo*, with some lamination, polarization, and distinct cell types [18-20]. Transplantation of post-mitotic progenitors or of a retinal sheet from organoid cultures into the mouse degenerative retina shows better although limited integration of the photoreceptors, which exhibit outer segment and synapse formation [21,22]. Thus, retinal organoids potentially offer a valuable platform to investigate retina development and disease and may provide a resource for regenerative medicine.

The optic cup formation and subsequent differentiation of retinal neurons are inefficient using the current protocols as less than 70% of the organoids produce optic vesicles (evagination of neuroepithelia) at day (D)7 and only 18–35% generate optic cups (subsequent invagination of optic vesicles) by D10 [18,19,23,24]. Using most protocols, the neural retina in organoid cultures survives for approximately 25 days and exhibits limited development of inner retina neurons and a relatively smaller number of rod photoreceptors [21,23-25]. iPSCs derived from rods (compared to fibroblasts) exhibit higher efficiency of differentiation [25]; however, such a scenario might not be possible for human therapy.

The purpose of this study is to achieve high-efficiency differentiation of stem cells into retinal organoids, which recapitulate *in vivo* retinogenesis and include 70–75% of rod photoreceptors. To examine rod differentiation directly, we generated ESC and iPSC lines from *Nrl*-GFP mice, in which green fluorescent protein (GFP) expression is controlled by the promoter of the neural retina leucine zipper transcription factor *Nrl* [26]. As *Nrl* determines the fate of the rod cells [27,28] and is the first rod lineage-specific marker [29], rod birth and subsequent differentiation can be followed with GFP expression. Using modified culture conditions (High Efficiency Hypoxia Induced Generation of Photoreceptors in Retinal Organoids, HIPRO), the retinal organoids from *Nrl*-GFP ESCs and iPSCs exhibited longer survival, high differentiation efficiency, and better stratification with the development of inner retina neurons. The rod photoreceptors in the retinal organoids at D35 accounted for almost 70% of all cells, and the rod photoreceptors' transcriptome appeared similar to that reported for P6 rods from the mouse retina [30]. The retinal organoid cultures, we report, thus provide a useful model for investigating early photoreceptor development, modeling degenerative disease, and exploring novel treatment paradigms.

## METHODS

*Generation and maintenance of ESCs and iPSCs from Nrl-GFP mice:* ESC and iPSC clones were derived based on published protocols [31,32]. In brief, ESC clones were isolated from the inner cell mass (ICM) of 3.5-day blastocysts of *Nrl*-GFP transgenic mice on feeders of mouse embryonic fibroblast (MEF) in the presence of leukemia inhibitory factor (LIF; Millipore, Darmstadt, Germany) and 3i [33] and maintained under the same conditions at 37 °C in a humidified environment of 5% $CO_2$. iPSC clones were generated by infection of the E14.5 MEFs from *Nrl*-GFP mice of Dox-inducible lentiviral vectors carrying *Oct3/4*, *Sox2*, *Klf4,* and *c-Myc* genes individually and then cultured on MEF feeder cells for 3 weeks. Embryonic stem cell–like colonies were picked and transferred onto fresh feeder cells, followed by evaluation of quality by morphology, proliferation rate, and Nanog expression. *Nrl*-GFP ESCs and iPSCs were maintained on feeder cells in knockout Dulbecco's Modified Eagle Medium (DMEM; Life Technologies, Carlsbad, CA, Catalog number: 11995073) supplemented with 1X Eagle′s minimum essential medium (MEM) non-essential amino acids (Sigma; St. Louis, MO, catalog number: M7145), 1X GlutaMAX (Life Technologies), 1X penicillin-streptomycin (PS; Life Technologies), 1×$\beta$-mercaptoethanol (Life Technologies), 2,000 U/ml Leukemia Inhibitory Factor (LIF; Millipore, Darmstadt, Germany), and 15% embryonic stem cell–qualified fetal bovine serum (FBS; Life Technologies). Cells were passaged using TrypLE Express (Life Technologies).

*Differentiation of Nrl-GFP ESCs and iPSCs into 3D neural retinas:* ESCs and iPSCs (passages 15–25) were differentiated using the SFEBq protocol [18] and after modifications in the culture conditions as follows: (i) The hypoxic condition was applied from D0 to D10; (ii) 36 uncut retinal organoids were cultured in a 100 mm Poly(2-hydroxyethyl methacrylate) (poly-HEMA)-coated (Sigma) dish after D14; (iii) $\beta$-mercaptoethanol was freshly added to the media every time; (iv) retinoic acid (RA; Sigma) was added to the culture from D14 to D26; (v) retinal organoids were supplied with DMEM/Nutrient Mixture F-12 (F12) with GlutaMAX (Life Technologies, catalog number: 10565042) supplemented with 2% FBS (Life Technologies), 1X penicillin-streptomycin (PS, Life Technologies), 1X MEM non-essential amino acid (NEAA, Sigma), 1X N2 supplement (Life Technologies), and 1X B27 supplement (Life Technologies); and (vi) 1X $\beta$-mercaptoethanol (Life Technologies) was added to all media every time. Then, 72 retinal organoids were transferred at D7 to a 100 mm poly-HEMA-coated Petri dish with 10 ml retinal maturation medium (DMEM/F12 with GlutaMAX with 1X PS). The maturation medium of the retinal cultures

was changed at D10, and 1 mM taurine and 500 nM RA were added. At D14, half of the media was changed and the culture density reduced to 36 organoids per 100 mm dish. The cultures were maintained until D26 with half of the media changed every 3 days. At D26, the full media were replaced with DMEM/F12-containing GlutaMAX that was supplemented with 2% FBS, 1X PS, 1X NEAA, 1X N2, and 1X B27. Half of the media was then changed every 2 days. The cultures were incubated at 5% $O_2$ from D0 to D10 and with 20% $O_2$ from D10 onward.

*Immunohistochemistry:* ESCs and iPSCs were plated into four-well Nunc® Lab-Tek® II Chamber Slides (Sigma) at a density of $56\times10^3$ cells per well. After 48 h, the cells were washed once with DPBS (Dulbecco's phosphate-buffered saline (DPBS, 2.6 mM KCl, 1.47 mM $KH_2PO_4$, 137.93 mM NaCl, 8.06 mM $Na_2HPO_4$-$7H_2O$, pH 7.0-7.3; Life Technologies, catalog number: 14190250) and fixed for 30 min using 4% paraformaldehyde (PFA; Electron Microscopy Science, Hatfield, PA). The cells were washed three times with DPBS and incubated for 1 h at room temperature in blocking solution containing DPBS with 10% FBS (Atlanta Biologicals, Flowery Branch, GA) and 0.2% Triton X-100 (Sigma). The cells were then incubated with anti-Nanog antibody (Mouse, 1:200 in blocking solution, ReproCELL, Kanagawa, Japan) overnight at 4 °C, followed by three washes of 5 min each with DPBS. Then 4',6-diamidino-2-phenylindole (DAPI; Life Technologies) and Alexa Fluor 568 anti-mouse antibody (1:250 in blocking solution, Life Technologies) were added, and the cells were incubated at room temperature for 1 h. After washing three times with DPBS (5 min each with gentle shaking), the cells were rinsed once with Ultrapure water (Life Technologies) to remove the sodium ions before the mounting solution was added. Fluorescence images were captured using the EVOS® XL system (Life Technologies).

For immunohistochemistry (IHC) of the differentiating neural retina, the organoids were fixed in 4% PFA (Electron Microscopy Science) for 1 h and cryoprotected in 15% sucrose for at least 2 h, followed by 30% sucrose overnight, before embedding in optimum cutting temperature (OCT) compound (Sakura Finetek, Torrance, CA). The OCT blocks were sectioned at 10 µm thickness and incubated at room temperature for at least 1 h, before immunostaining or storage at −80 °C. The immunostaining procedures have been recently described [20]. Primary antibodies were used at the following dilutions: laminin (rabbit, 1:50; Sigma), Zonula occludens-1 (ZO-1, rabbit, 1:100; Life Technologies), brain-specific homeobox/POU domain protein 3A (Brn3a, rabbit, 1:200; Santa Cruz, Dallas, TX), calbindin (Calb, rabbit, 1:1,000; Calbiochem, San Diego, CA), S-opsin (Opnsw, goat, 1:200; Santa Cruz), Prospero homeobox 1 (Prox1, rabbit, 1:200; Abcam, Cambridge, MA), Ceh-10 homeodomain-containing homolog (Chx10, sheep, 1:200; Abcam), protein kinase C alpha (PKCα, rabbit, 1:1,000; Sigma), GFP (chick, 1:500; Abcam), rhodopsin (Rho, mouse, 1:1,000; a gift from Dr. Robert Molday, University of British Columbia, Canada), glutamine synthetase (GS, rabbit, 1:200; Abcam), ADP-ribosylation factor-like protein 13B (Arl13b, rabbit, 1:1,000; Proteintech, Rosemont, IL), gamma-tubulin (γ-tubulin, mouse, 1:500, Sigma), and synaptophysin (mouse, 1:200, Abcam). Sections were incubated with the primary antibody at 4 °C overnight. Species-specific secondary antibodies, conjugated with Alexa Fluor 488 or 568, were diluted in antibody dilution buffer (1:250, Life Technologies) and incubated at room temperature for 1.5 h. DAPI (Life Technologies) was used for nuclear staining. For comparison of intensity, images in the same section were captured using identical gain and voltage. Fluorescence images were captured using an LSM 880 confocal microscope (Zeiss, Jena, Germany).

*FACS analysis:* ESCs and iPSCs were dissociated using TrypLE Express (Life Technologies). The cells were centrifuged at 180 ×g for 5 min and transferred to a T25 flask (Corning, Corning, NY) in 4 ml maintenance media to remove the feeder cells, which adhered to the flask in 20 min. Suspended cells were then fixed and stained with the FIX & PERM® Cell Fixation & Permeabilization Kit (Life Technologies) as suggested by the manufacturer. The cells were stained with anti-Nanog antibody overnight at 4 °C, followed by secondary antibody for 2 h at room temperature. The cells were then resuspended in DPBS containing 1 mM EDTA, filtered by 40 µm cell strainer (BD Bioscience, San Jose, CA), and kept on ice until fluorescence-activated cell sorting (FACS) analysis was performed using a MACSQuant Analyzer (Miltenyi Biotec, San Diego, CA).

For sorting the GFP+ cells, the retinal organoids were dissociated in 0.25% trypsin-EDTA (Life Technologies). The cells were centrifuged at 400 ×g for 5 min, resuspended in DPBS containing 1 mM EDTA, and filtered with a 40 µm cell strainer (BD Bioscience). The samples were kept on ice until sorting with FACSAriaII (BD Bioscience). Cell viability was evaluated by integrity (gated by DAPI) and size (gated by forward scatter, FSC). Gating of GFP+ cells was based on wild-type retinal organoids without GFP at the same differentiation day.

*RNA extraction and RT–PCR:* Total RNA was purified from tissue homogenates or flow-sorted GFP+ photoreceptors using TriPure isolation reagent (Roche, Basel, Switzerland). RNA quantity was assessed with a NanoDrop 1000 spectrophotometer (Thermo Scientific, Rockville, MD). Reverse

Table 1. Sequence of primers used for RT–PCR.

| Gene | | Product, bp | Sequence |
|---|---|---|---|
| *Gapdh* | Forward | 212 | TGTTGCCATCAATGACCCCTT |
| | Reverse | | CTCCACGACGTACTCAGCG |
| *Pax6* | Forward | 252 | AAGGAGGGGGAGAGAACACC |
| | Reverse | | ATTTGGCCCTTCGATTAGAA |
| *Rax* | Forward | 253 | ATCCCAAGGAGCAAGGAGAG |
| | Reverse | | TTCTGGAACCACACCTGGAC |
| *Nrl* | Forward | 116 | TTTGGAGGTGGCTGGGTAGATG |
| | Reverse | | ACGATGCTCAGAAGTTTGGGG |
| *Rho* | Forward | 139 | CCCTTCTCCAACGTCACAGG |
| | Reverse | | TGAGGAAGTTGATGGGGAAGC |

transcription (RT) was performed using a SuperScript III Reverse Transcription-PCR kit (Life Technologies) and complementary DNA (cDNA) was generated using oligo(dT) primer. The resulting cDNA was amplified using gene-specific primers (Table 1). PCR products were separated by 1% agarose gel (Lonza, Walkersville, MD) and detected under ultraviolet (UV) illumination (PerkinElmer, Waltham, MA).

*Transcriptome analysis:* RNA sequence (RNA-seq) profiles of high-quality total RNA (RNA integrity number ≥7.5) from the GFP+ photoreceptors were obtained using the Illumina platform. These paired-end RNA-seq data were compared to reported single-end mouse rod transcriptome [30] as follows. After the Illumina adapters were trimmed, defined in the TruSeq3-PE-2.fa file, by Trimmomatic (version 0.36) [34] from paired-end data, each sample was quantified against Ensembl release 84 [35] cDNA FASTA file by Kallisto (version 0.42.5) [36] via a custom pipeline in Perl (Perl version 5.16.3). The quantifications were then normalized and summarized at the gene level with tximport [37] with the option "countFromAbundance=lengthScaledTPM." The statistical environment R (version 3.3.1) installed on a 64-bit GNU Red Hat Linux system (Centos 7.2) was used to further analyze the data and to generate heatmaps. The count values from tximport were converted to count per million (CPM) via edgeR [38]. Logarithmically transformed (base 2) CPM values were used for the PCA and clustering. All GFP+ data were averaged for each time point to avoid replicates. The heatmap function has been used previously [20]. Photoreceptor genes data were clustered with the affinity propagation algorithm [39] using the negative distance matrix option as the similarity measure. PCA analysis was performed with custom plotting, using prcomp function in R without scaling and centering the data. To highlight the time matching, the first principal component was plotted against the 11$^{th}$ component on the x- and y-axes, respectively.

*Statistical analysis:* All data were expressed as mean ± standard error of the mean (SEM), unless specified. An unpaired two-tailed Student *t* test was used to compare the mean between two groups. Results with a p value of less than 0.05 were considered statistically significant. At least three independent biologic replicates were performed (n = number of experiments).

## RESULTS

*Characterization of ESCs and iPSCs from Nrl-GFP mice:* *Nrl*-GFP ESCs and iPSCs were evaluated by the morphology, proliferation rate, and expression of Nanog, which is a critical transcription factor for pluripotency [40]. There was no significant difference between the ESCs and iPSCs in terms of morphology (Figure 1A) and proliferation rate (Figure 1B), both of which were consistent with other publications [41,42]. Nanog expression was detected in the nuclei of all ESC and iPSC colonies (Figure 1C). Flow analysis showed that all ESCs and iPSCs were pluripotent and exhibited Nanog expression (Figure 1D).

*Efficient generation of optic vesicles and optic cups from mouse ESCs and iPSCs:* The SFEBq protocol was modified to efficiently obtain a more mature neural retina by changing the oxygen level and medium components during differentiation (Figure 2A). Oxygen tension has been demonstrated to impact the viability and cell fate commitment of neurons during early neuronal development in mice and humans [43,44]. Thus, the hypoxic condition was applied from D0 to D10 in the modified protocol. Under normoxia (20% $O_2$) and hypoxia (5% $O_2$) conditions, mouse ESCs and iPSCs could be differentiated into embryoid bodies with a neuroepithelium at D4, an optic vesicle at D7, and an optic cup at D10, without

significant morphological differences (Figure 2B). To assess the efficiency, differentiating organoids with optic vesicle and optic cup formation were quantified at D7 and D10, respectively. Organoids in hypoxic condition demonstrated significantly higher differentiation into optic vesicles and optic cups (Figure 2C). For ESCs and iPSCs, more than 70% of the organoids formed optic vesicles by D7 (n = 10, range from 50% to 95%), and more than 50% formed optic cups on D10 (n = 10, range from 30% to 85%), compared with 40% at D7 (n = 10, range from 30% to 50%) and less than 20% (n = 10, range from 8% to 30%) at D10 with the original SFEBq method. To avoid bias in counting, 60 organoids at D10 were randomly selected and harvested for RNA. RT–PCR analysis was performed to measure the expression of early eye field transcription factors. As predicted, the embryoid bodies under hypoxic conditions revealed higher expression of Pax6 and Rax, suggesting commitment to the retinal cell fate by a greater number of cells (Figure 2D).

*Polarization of the neural retina and genesis of early-born neurons:* To investigate whether the neural retinas generated by the modified protocol mimic the *in vivo* mouse retina in terms of polarity, lamination, and the presence of all cell types, immunostaining was performed using various retinal markers. Apical-basal polarity of the neural retina is critical for the proper functioning of photoreceptors [45]. The neural retinas generated using the modified protocol revealed polarity, with the outer side basal and the inner side apical (Figure 3A).

Ganglion cells and horizontal cells are the two earliest-born cell types in 3D retinas, as evident by the expression of Brn3a and calbindin (Calb), respectively (Figure 3B). As early as D14, ganglion cells could be detected at the basal side of the neural retina, with a substantial increase in the number at D18. However, the number of ganglion cells decreased at D21, which may be due to the lack of axon formation or other secretory factors from the brain in culture [46,47]. Horizontal cells started to be born at D14, and few cells were detected

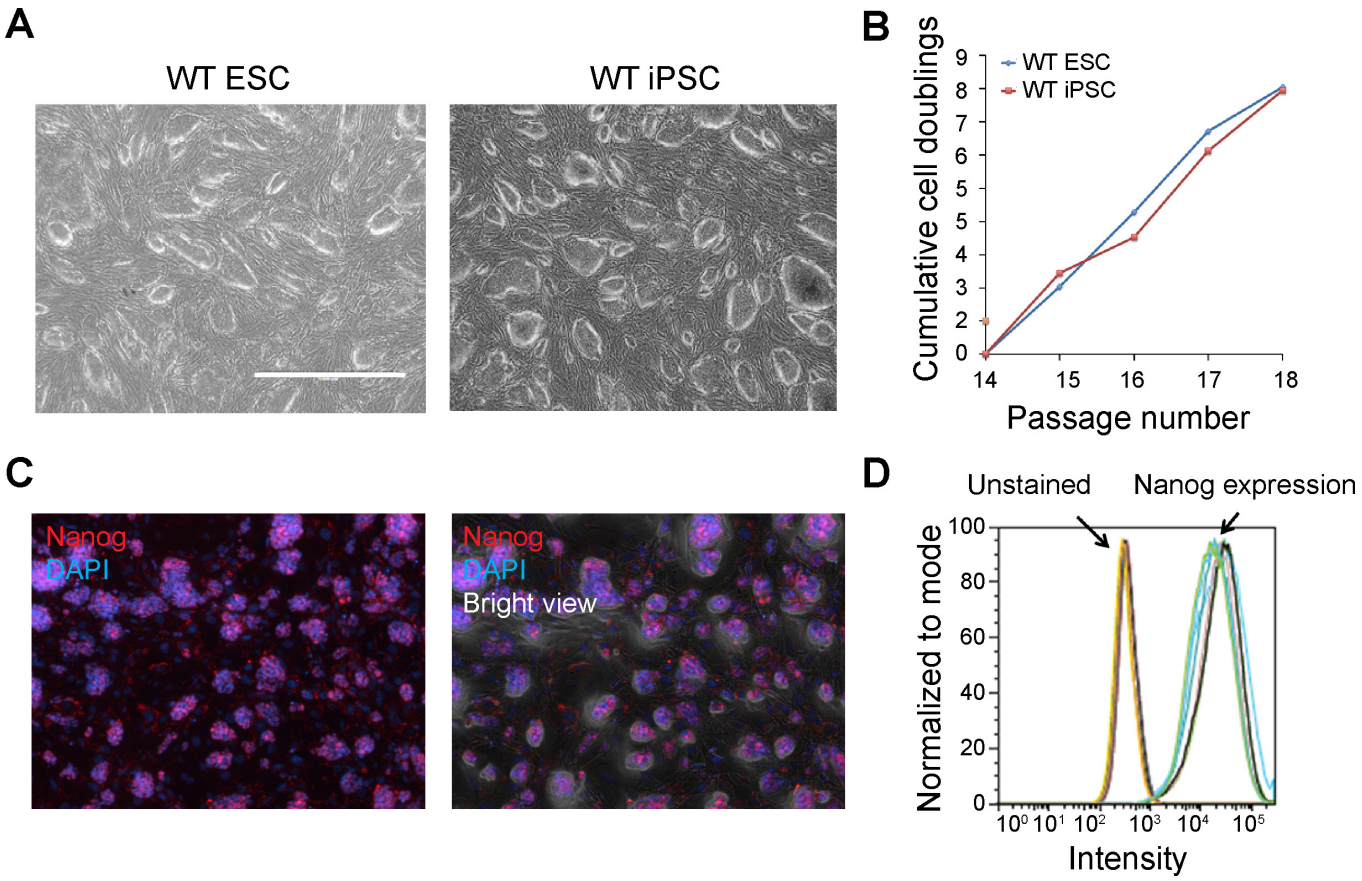


Figure 1. Characterization of mouse ESCs and iPSCs. (**A**) morphology, (**B**) proliferation rate, (**C**) expression of pluripotency marker Nanog, and (**D**) percentage of Nanog+ cells. No significant morphological differences were observed between the embryonic pluripotent stem cells (ESCs) and the induced pluripotent stem cells (iPSCs). Nanog staining is representative of both stem cell types. Nuclei were stained with 4',6-diamidino-2-phenylindole (DAPI; blue). Scale bar = 100 µm.

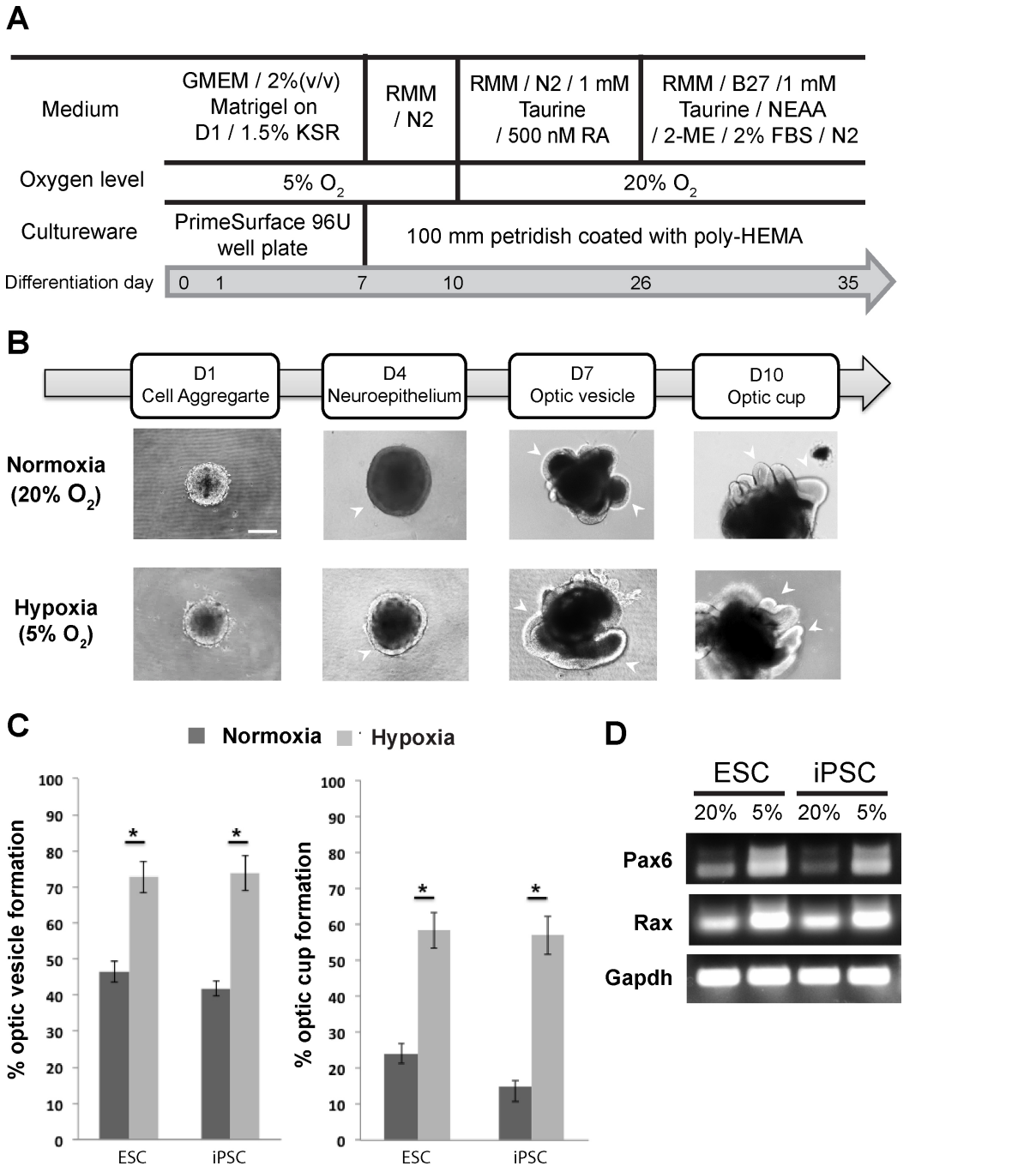


Figure 2. Generation of retinal organoids from *Nrl*-GFP mouse ESCs and iPSCs. **A**: Schematic representation of the High Efficiency Hypoxia Induced Generation of Photoreceptors in Retinal Organoids (HIPRO) protocol for differentiation of mouse stem cells into the three-dimensional (3D) neural retina. GMEM, Glasgow minimum essential medium; KSR, knockout serum replacement; poly-HEMA, polyhydroxyethylmethacrylate; RMM, retinal maturation medium constituted of DMEM/F12 with GlutaMAX, 1X penicillin-streptomycin, and 1X $N_2$ supplement; RA, retinoic acid; FBS, fetal bovine serum; N2, N2 supplement; B27, B27 supplement. **B**: Morphology of organoids at different time points using normoxic and hypoxic conditions. **C**: Percentage of organoids that form optic vesicles at day (D)7 and optic cups at D10. Optic vesicles are defined as protrusions of neuroepithelia from the organoids. Optic cups are characterized by a hinge region due to inward folding of the neuroepithelia of the optic vesicles. The data were obtained from ten independent experiments (n = 10, each had a total of 144 organoids) and represented as mean ± standard error of the mean (SEM); *$p<0.05$. **D**: Reverse transcription PCR (RT–PCR) analysis of early eye field transcription factors (*Pax 6* and *Rax*) using total RNA from D10 organoids (60 organoids derived from embryonic pluripotent stem cells (ESCs) or 60 organoids from induced pluripotent stem cells (iPSCs)). *Gapdh* was used as a control.

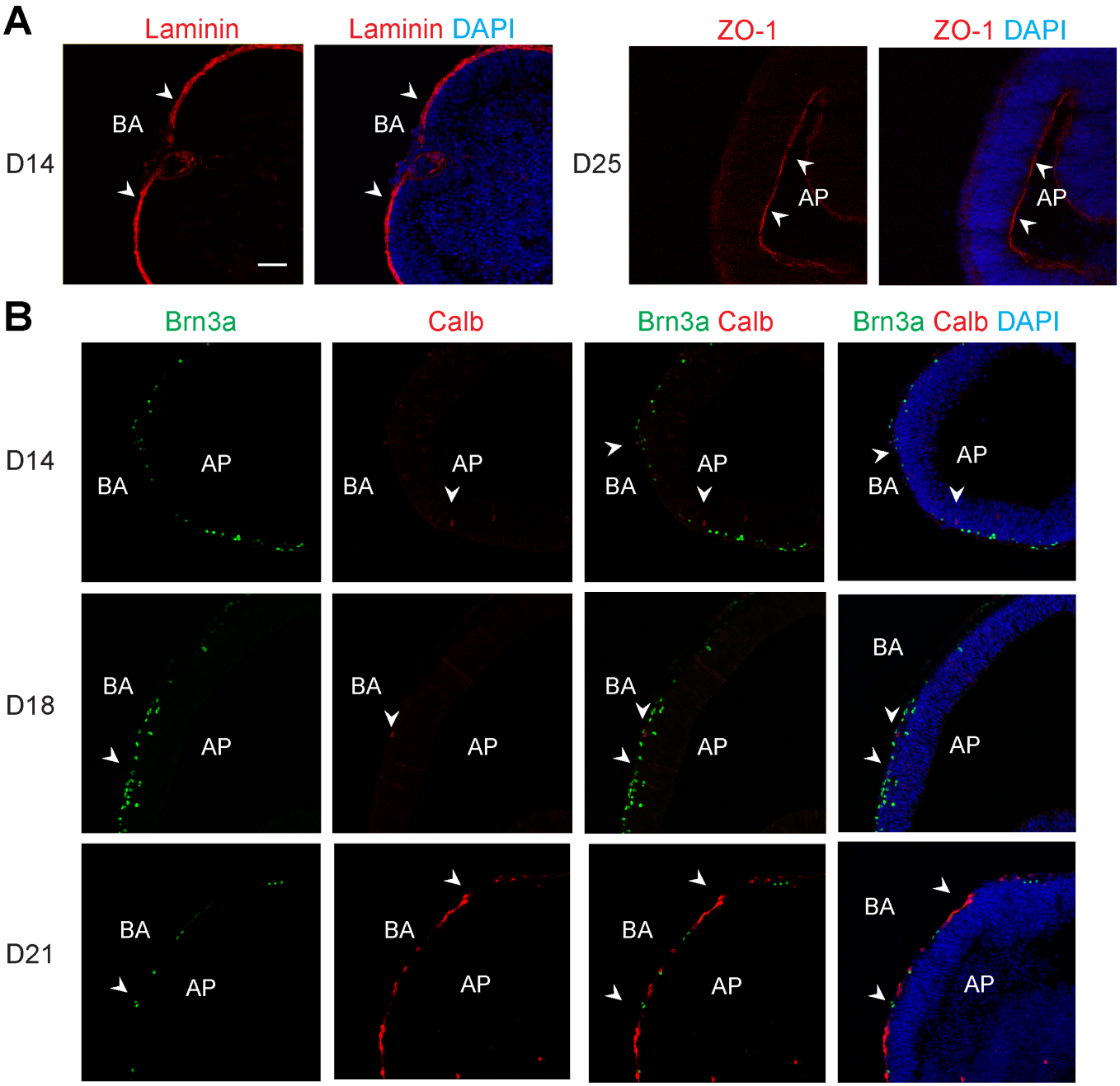


Figure 3. Differentiation of early-born cell types in the polarized neural retina. AP and BA show the apical and basal sides of the organoid, respectively. Nuclei were stained with 4',6-diamidino-2-phenylindole (DAPI; blue). No significant morphological differences were observed among the neural retinas differentiated from the embryonic pluripotent stem cells (ESCs) or induced pluripotent stem cells (iPSCs); representative figures are shown. Arrowheads indicate relevant immunostaining with organoid polarity in (**A**), and Brn3a and Calb in (**B**). **A**: Polarity of the three-dimensional (3D) retina at day (D)14 and D25. Laminin (red) and ZO-1 (red) are basal and apical markers, respectively. **B**: Development of ganglion cells (Brn3a, green) and horizontal cells (Calbindin, Calb, red) in the D14 to 21 retinal organoids. NBL, neuroblastic layer; ONL, outer nuclear layer; INL, inner nuclear layer; GCL, ganglion cell layer. Scale bar = 50 µm.

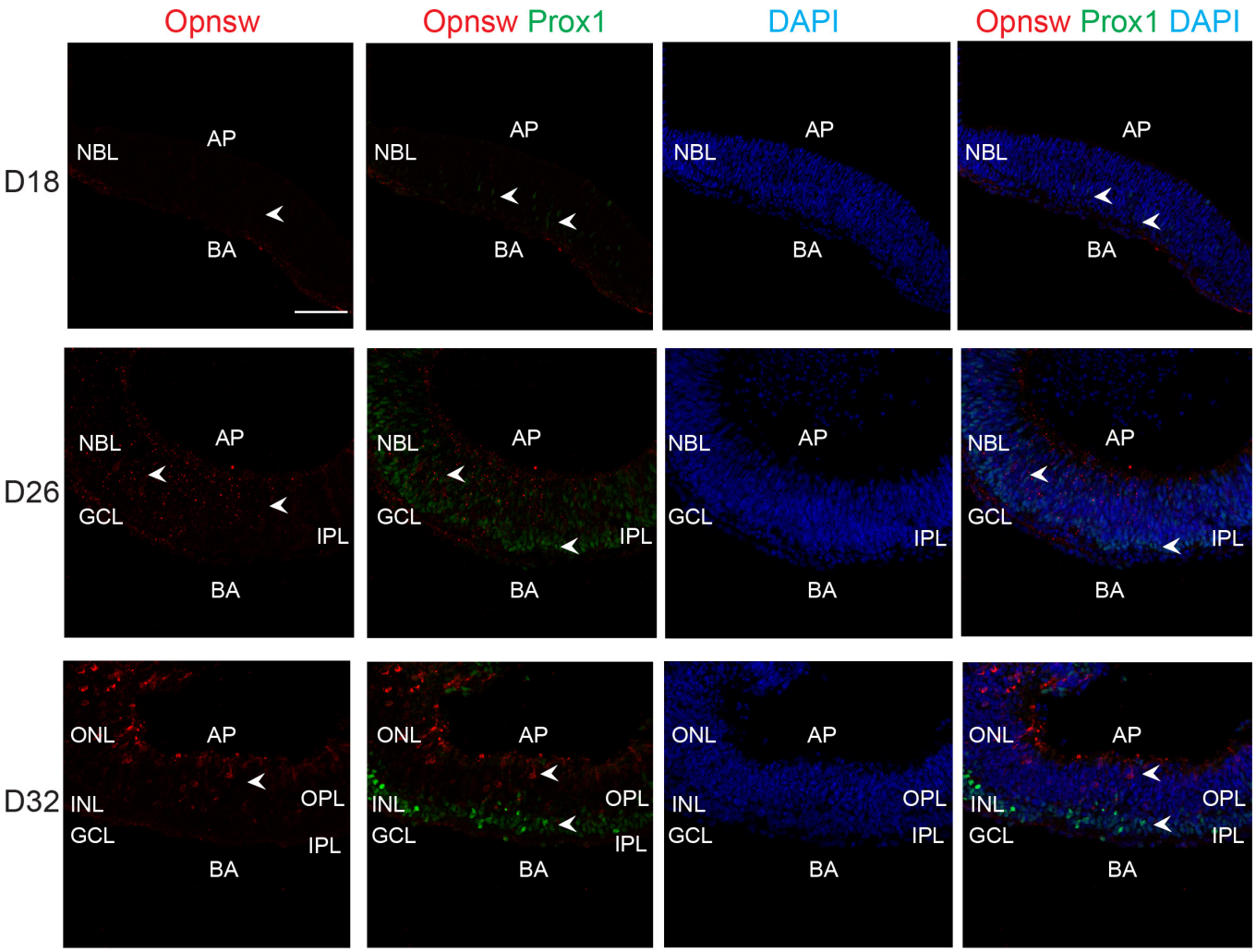


Figure 4. Development of cone photoreceptors and amacrine cells, followed by the formation of plexiform layers. Immunostaining with S-opsin (Opnsw, red) and Prox1 (green) antibodies shows S-cones and amacrine cells, respectively. No significant morphological differences were observed among the neural retinas differentiated from embryonic pluripotent stem cells (ESCs) or induced pluripotent stem cells (iPSCs); representative figures are shown. Arrowheads indicate the relevant immunostaining with Opnsw and Prox1. AP and BA show the apical and basal sides of the organoid, respectively. NBL, neuroblastic layer; ONL, outer nuclear layer; INL, inner nuclear layer; GCL, ganglion cell layer. Nuclei were stained with 4',6-diamidino-2-phenylindole (DAPI; blue). Scale bar = 50 µm.

at the middle part of the neural retina. At D18, the horizontal cells migrated to the basal side, and their number greatly expanded at D21, with limited connections among the cells.

The birth of ganglion cells and horizontal cells is followed by the generation of cone photoreceptors and amacrine cells (Figure 4). At D18, cones and amacrine cells were detected with minimal expression of S-opsin (Opnsw) and Prox1, respectively, at the middle part of the neuroblastic layer (NBL). At D26, cone cells were found at the apical side of the NBL, while amacrine cells were mainly located at the basal side. With the development of amacrine cells, the inner plexiform layer (IPL) started to form at this stage. Further maturation of the cone photoreceptors and amacrine cells was indicated by the significant increase in expression of Opnsw and Prox1, respectively. At D32, the cone photoreceptors had typical morphology and were located in the outer nuclear layer (ONL), which is at the apical side of the neural retina. Notably, the outer plexiform layer (OPL) and the IPL were detected at this stage. Most amacrine cells were located at the inner nuclear layer (INL), with some misplaced at the ganglion cell layer (GCL).

The *Nrl*-GFP ESC and iPSC lines were also differentiated using the original SFEBq protocol for comparison (Appendix 1). At D26, the inner retina neurons were not fully developed, and only the NBL and the GCL could be observed.

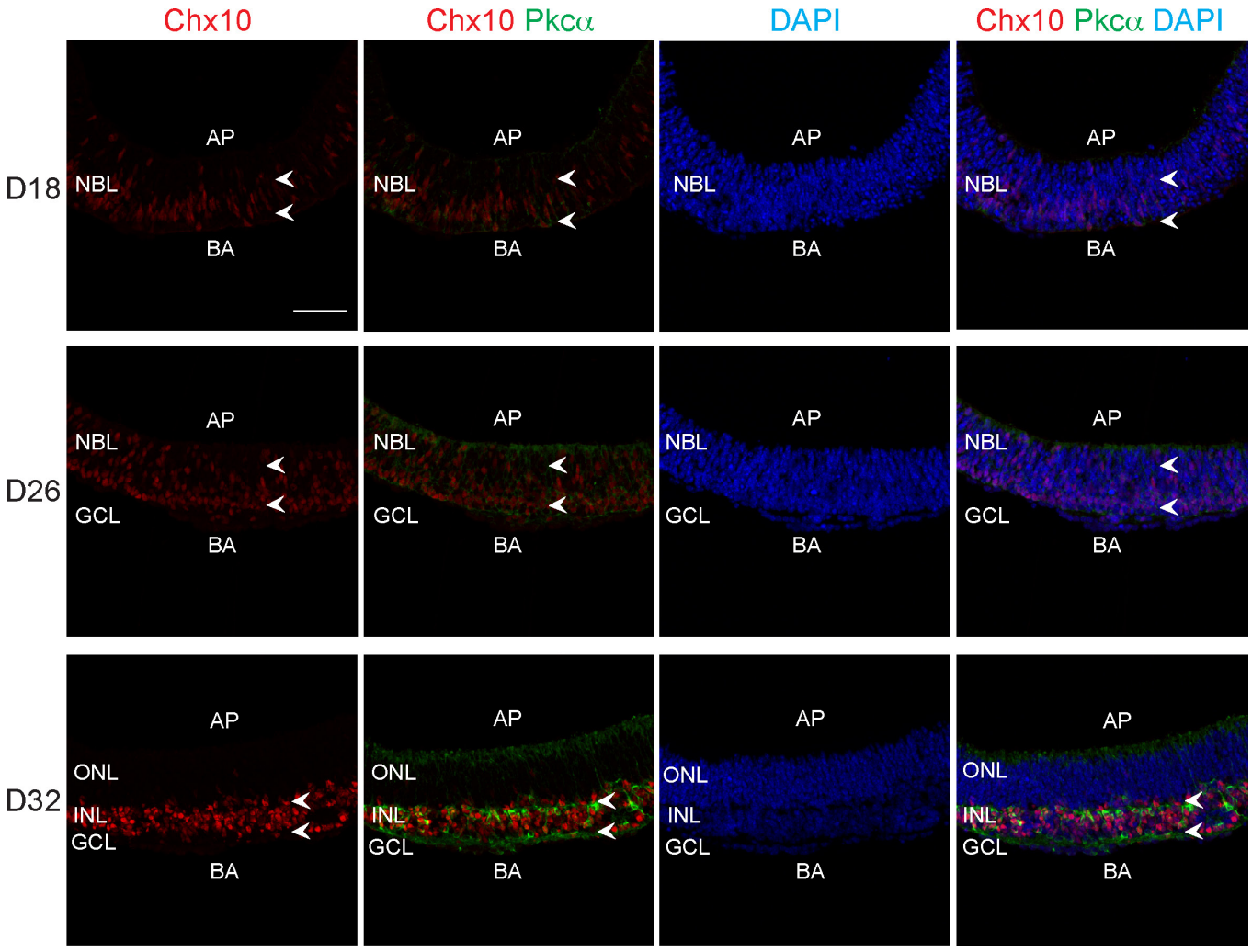


Figure 5. Genesis of bipolar cells in retinal organoids at different stages of differentiation (day (D)18 to D32). Ceh-10 homeodomain-containing homolog (Chx10; red) is a marker of proliferating cells as well as differentiated bipolar cells. Protein kinase C alpha (PKCα; green) is a marker of ON-bipolar cells. No significant morphological differences were observed among the neural retinas differentiated from embryonic pluripotent stem cells (ESCs) or induced pluripotent stem cells (iPSCs); representative figures are shown. Nuclei were stained with 4',6-diamidino-2-phenylindole (DAPI; blue). Arrowheads indicate the relevant immunostaining in the inner retina. At D18 and D26, the Chx10 labeling shows mostly proliferating cells. AP and BA show the apical and basal sides of the organoid, respectively. NBL, neuroblastic layer; ONL, outer nuclear layer; INL, inner nuclear layer; GCL, ganglion cell layer. Scale bar = 50 µm.

The morphology of the neural retina in these experiments was similar to that reported by others [23,24,48].

*Development of bipolar neurons:* During *in vivo* retinal development, formation of the OPL and the IPL is followed by the development of bipolar cells to connect the two plexiform layers [49]. Chx10 is a marker for proliferative cells or bipolar cells, depending on the differentiation stage. At an early stage of differentiation (D18), proliferative cells were found throughout the NBL, as indicated by Chx10 staining. As the cells started to commit bipolar cell fate, a small portion of Chx10+ cells were located at the basal side of the NBL at D26, while most remained in the NBL, which were proliferative retinal progenitor cells. With further maturation of the neural retina, all cells exited the cell cycle at D32, and Chx10+ cells were detected only at the ONL, indicating the proper location of bipolar cells. PKCα is the marker for ON-bipolar cells, and its expression indicates the maturation of bipolar cells. A substantial expression of PKCα was detected only in the late stage of differentiation, connecting the OPL and the IPL (Figure 5).

*Differentiation of rod photoreceptors and Müller glia: Nrl* is the earliest marker of post-mitotic rods; *Nrl* expression is detected at rod birth, followed by *Rho* expression as the differentiation proceeds [26,29]. RT–PCR analysis of the

neural retina showed that *Nrl* expression began at D15, with a continuous increase during differentiation (Figure 6A). A minimal amount of *rhodopsin* (*Rho*) expression was detected at D18 and increased with time as the rod photoreceptors matured (Figure 6A). As GFP is under the control of the *Nrl* promoter in ESCs and iPSCs, differentiating cells committed to rod cell fate would express GFP in organoids. Flow analysis of the dissociated organoids revealed a progressive increase in GFP+ cells and in the intensity of GFP (Figure 6B). Notably, the GFP+ rod cells constituted more than 70% of the total population at D35, closely mimicking the mature mouse retina *in vivo* [26] (Figure 6C). At D18, there were few GFP+ cells with weak signal intensity, but more GFP+ cells with higher intensity were detected by D21 (Figure 6B,D). After D25, GFP seemed polarized to the apical side of the neural retina, with D35 having the highest GFP+ cell number and signal intensity (Figure 6D). Thus, the retinal organoids generated by the HIPRO protocol demonstrated longer survival and more GFP+ rods compared to the original SFEBq protocol (Appendix 1).

Most rod photoreceptors and Müller glia are born postnatally in the mouse retina [50]. At D18, rod photoreceptors were evident by the minimal expression of Reep6, a marker for rod photoreceptors [51], at the apical side of the neural retina. Expression of Reep6 increased at D25, indicating the maturation of the rods. In addition, GS, a marker for Müller glia, was mainly located at the basal side, while Reep6 was polarized to the apical side. From D32 and onward, the Müller glia matured further and spanned the entire neural retina, and the outer limiting membrane (OLM) was evident at the apical side of NR, with Reep6 protruding beyond the OLM. With the HIPRO protocol, the organoid cultures were maintained until D35, with an intact structure of the neural retina (Figure 7).

*Genesis of photoreceptor cilium and synaptic morphology:* Photoreceptor outer segments originate as modified primary cilium [52,53], and limited ciliogenesis has been one of the shortcomings of 3D retinal organoid cultures [18,19,21,54]. Using the HIPRO protocol, we facilitated cilia growth in retinal organoids and detected elongation of the ciliary axoneme at the apical side of the neural retina (Figure 8A). At D25, basal bodies, indicated by immunostaining of γ-tubulin, were polarized to the apical side of the neural retina, suggesting the start of ciliogenesis. At this stage, immunostaining of ADP-ribosylation factor-like protein 13B (Arl13b), a marker of ciliary axoneme, was barely detectable. As the photoreceptors continued to mature, more cells with elongated cilium were observed at D32, as indicated by

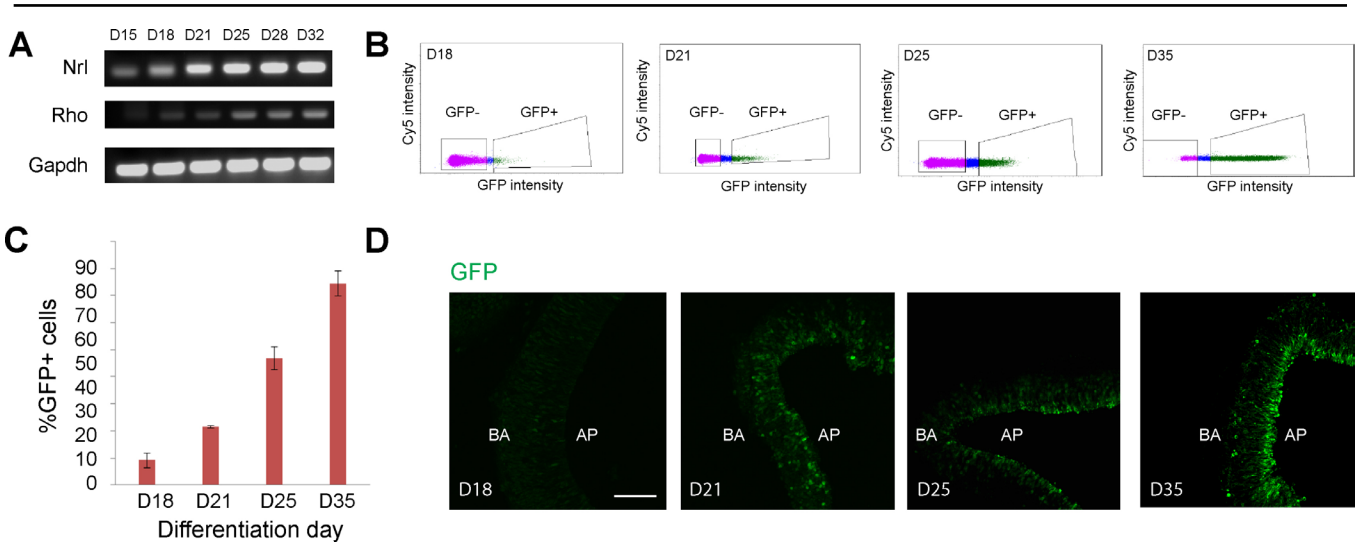


Figure 6. Generation of rod photoreceptors in *Nrl*-GFP mouse retinal organoids. **A**: Time course of *Nrl* and rhodopsin (*Rho*) expression during organoid differentiation with reverse transcription PCR (RT–PCR). Total RNA was made from 20 dissected neural retinas. *Gapdh* expression was used as the control. **B**: Dot plots of flow analysis of GFP+ cells during organoid differentiation. Gating of GFP+ cells was based on wild-type retinal organoids without green fluorescent protein (GFP) at the same differentiation day. **C**: The bar chart shows the percentage of GFP+ cells (rods) in the total cell population. No significant differences were observed in the percentage of GFP+ cells from embryonic pluripotent stem cells (ESCs) or induced pluripotent stem cells (iPSCs)–derived retinal organoids. The data are represented as mean ± standard error of the mean (SEM) and were obtained from four independent experiments each from ESC and iPSC organoids (n = 4). Each experimental time point included 30–60 organoids. *$p<0.05$. **D**: GFP (green) expression in retinal organoids at different stages of differentiation. No significant morphological differences were observed among the neural retinas differentiated from ESCs or iPSCs; representative figures are shown. AP and BA show the apical and basal sides of the organoid, respectively. Scale bar = 100 µm.

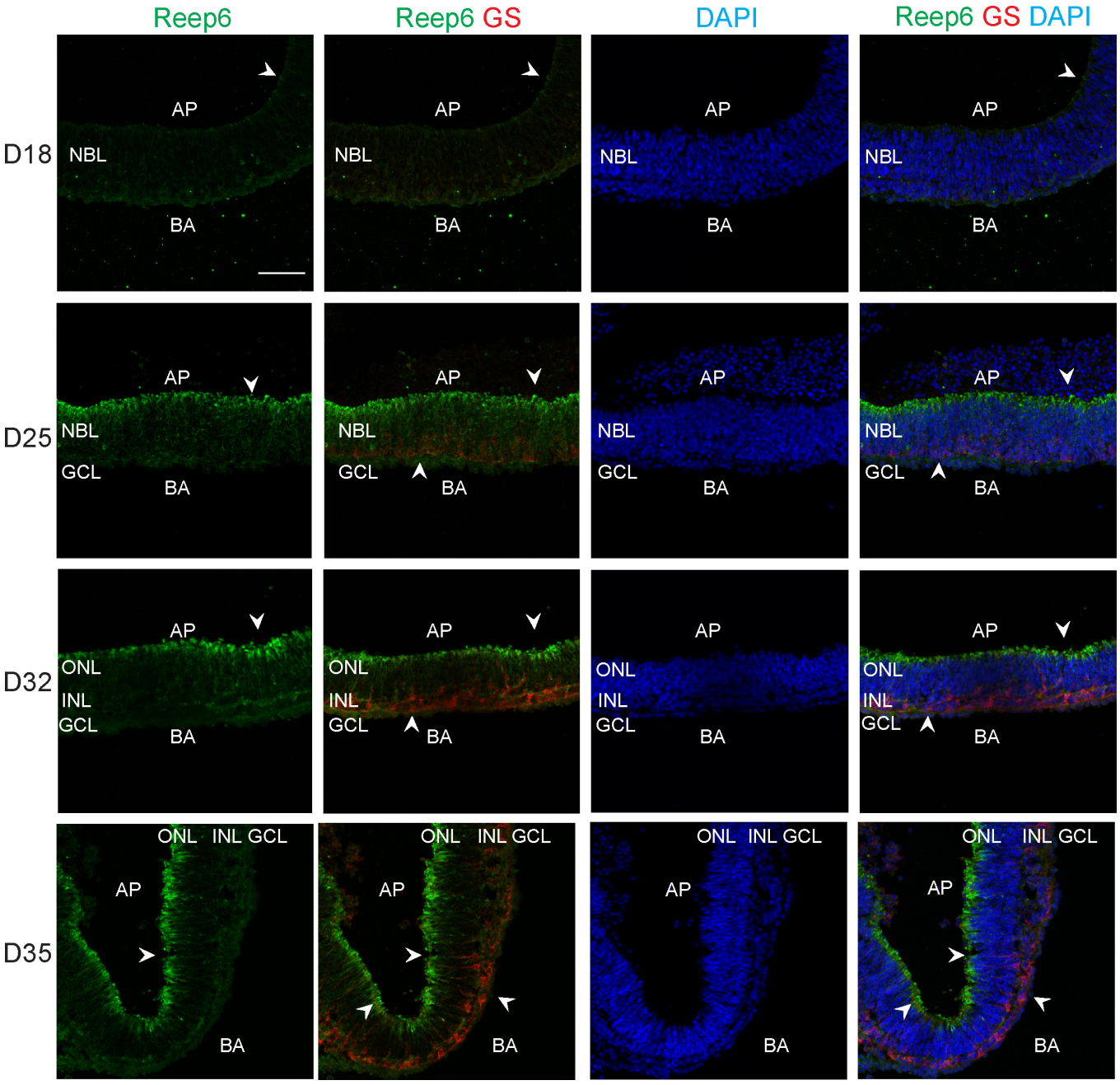


Figure 7. Differentiation of rod photoreceptors and Müller glia in developing retinal organoids (day (D)18–35). Reep6 (green) and glutamine synthetase (GS, red) are markers of rod photoreceptors and Müller glia, respectively. No significant morphological differences were observed among the neural retinas differentiated from embryonic pluripotent stem cells (ESCs) or induced pluripotent stem cells (iPSCs); representative figures of the neural retinas are shown. Nuclei were stained with 4',6-diamidino-2-phenylindole (DAPI; blue). Arrowheads indicate the relevant immunostaining with Reep6 and GS. AP and BA show the apical and basal sides of the organoid, respectively. NBL, neuroblastic layer; ONL, outer nuclear layer; INL, inner nuclear layer; GCL, ganglion cell layer. Scale bar = 50 µm.

Arl13b. Colabeling with Rho and Arl13b demonstrated their partial colocalization, with Rho immunostaining extending beyond Arl13b, suggesting the initiation of outer segment biogenesis (Figure 8B).

In addition, we observed the formation of plexiform layers, as indicated by synaptophysin immunostaining. At D26, only the IPL was detected with a trace amount of synaptic vesicles. As the development proceeded, the OPL was detected with significant labeling with synaptophysin. Increased synaptic staining was also detected in the IPL at D32, suggesting further maturation of the INL cell types (Figure 8C).

*Gene profiling:* After the transcriptome data from the GFP+ rods derived from the D25, D28, and D35 organoids were normalized with the published RNA-seq of the developing mouse rods [30], we applied PCA to the whole data set (Figure 9A). The principal component 1 (PC1) captured more than 30% of all variations in the data and perfectly captured the variance between time points. The PCA plot showed that the D25 and D28 data coprojected on PC1 with the P2 and P4 time points of the mouse rods, whereas D35 falls between P6 and P10 but closer to the P6 developmental stage. A heatmap showing the expression profiles of the photoreceptor genes validated the PCA results and further demonstrated that the

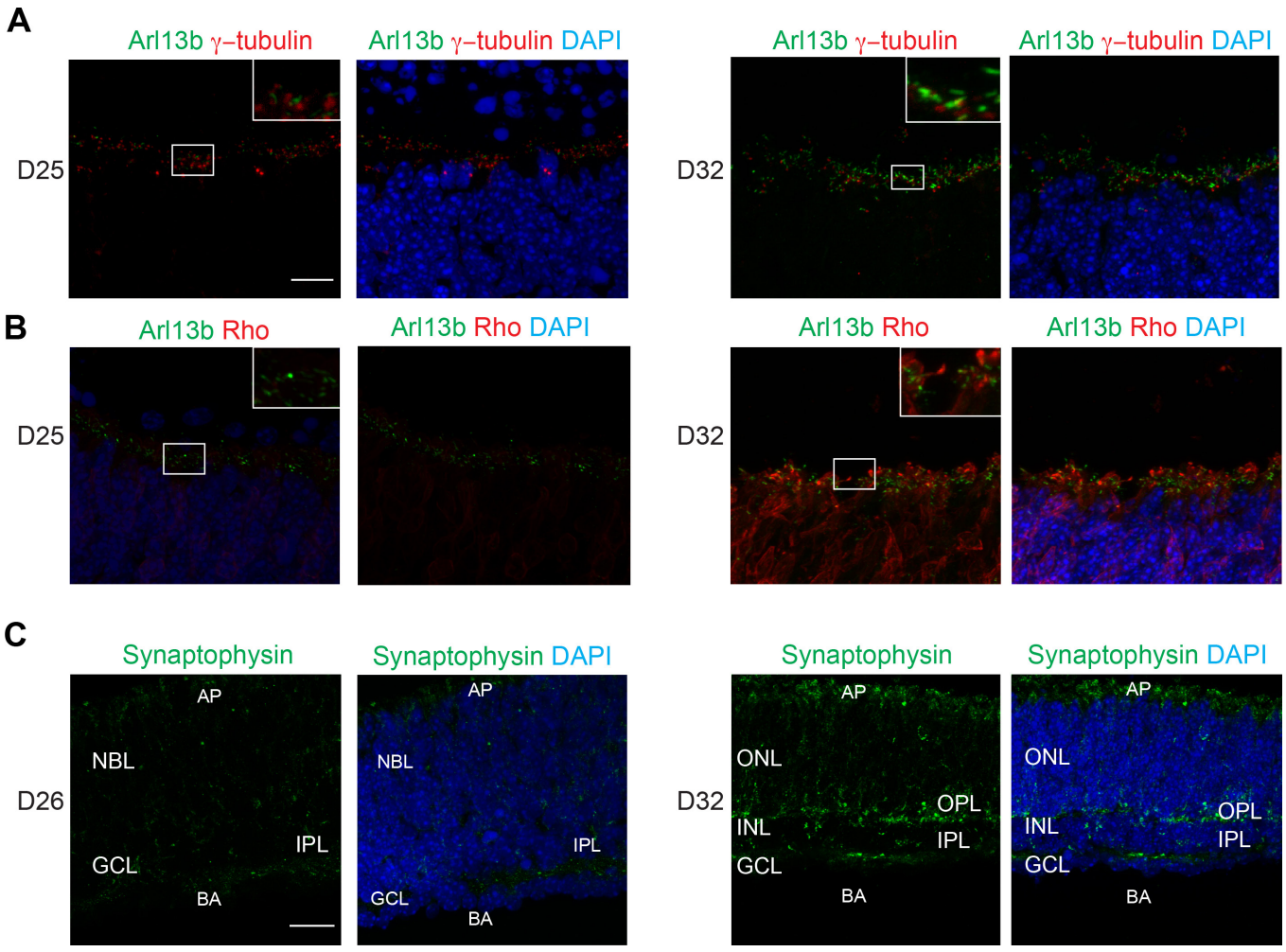


Figure 8. Maturation of photoreceptors and synaptic layers in the retinal organoids (day (D)25–32). No significant morphological differences were observed among the neural retinas differentiated from embryonic pluripotent stem cells (ESCs) or induced pluripotent stem cells (iPSCs); representative figures of the neural retinas are shown. Nuclei were stained with 4',6-diamidino-2-phenylindole (DAPI; blue). **A**: Appearance of photoreceptor cilia. Gamma-tubulin (γ-tubulin, red) is a marker of basal bodies, whereas ADP-ribosylation factor-like protein 13B (Arl13b, green) stains the ciliary axoneme of photoreceptors. **B**: Labeling of rhodopsin (Rho, green) beyond Arl13b (red) staining. **C**: Synaptophysin (green) labeling indicates the synaptic layers. The white rectangles show higher magnification images of the selected region. AP and BA show the apical and basal sides of the organoid, respectively. NBL, neuroblastic layer; ONL, outer nuclear layer; INL, inner nuclear layer; GCL, ganglion cell layer. Scale bar = 10 µm.

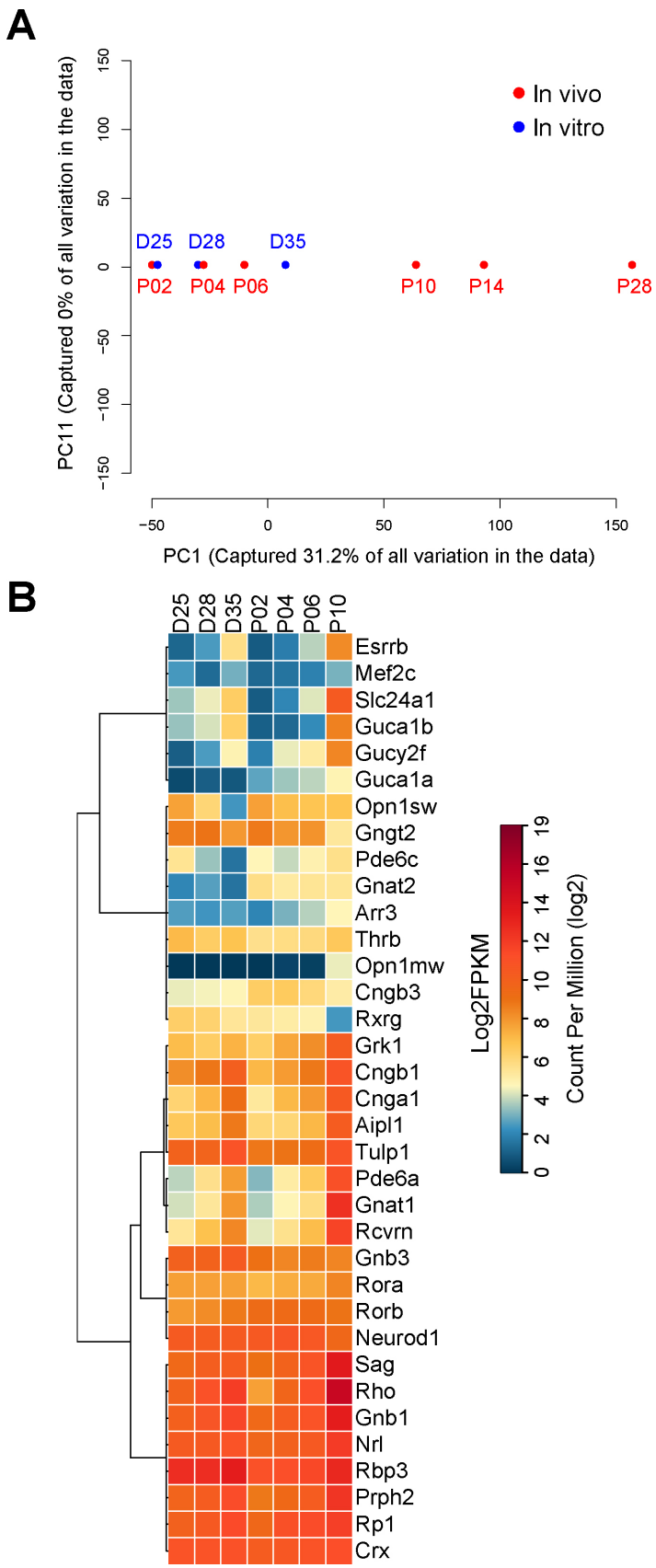


Figure 9. A comparison of *in vitro* and *in vivo* rod photoreceptor differentiation. D25, D28, and D35 represent the days in culture for the retinal organoids, and P2–10 correspond to the postnatal day mouse retina. **A**: The principal component analysis (PCA) plot shows the transcriptome data for purified rods from the *Nrl*-GFP organoid culture and from the mouse retina. PC1 (on the x-axis) shows that the largest component of the variance in the expression data (31.2%) is due to the developmental time. **B**: The heatmap shows the expression of the photoreceptor genes in the developing rods from the organoid culture and the mouse retina.

D35 rods in the organoid culture were more mature than in the P6 retina (Figure 9B). Notably, the developing rod photoreceptors in the retinal organoids also expressed cone genes, consistent with the proposed concept of the potential origin of mammalian rods from S-cones [30].

## DISCUSSION

Here, we described a modified differentiation protocol, called HIPRO, for mouse retinal organoid culture, with efficient production of a more mature neural retina mimicking *in vivo* retinogenesis. A striking observation in the study is the efficient generation of optic vesicles and optic cups by applying hypoxic conditions to organoid cultures from D0 to D10. The efficiency of optic cup formation is reportedly low under normoxic condition [18,23-25], except in one study that demonstrated high efficiency of optic cup formation by maintaining Matrigel until D10 instead of D7 [21]. Although differentiation efficiency varies among clones and batches [22], the concurrent comparison of organoids derived from ESCs and iPSCs in the present study showed a significant improvement in optic cup formation when hypoxic conditions are provided from D0 to D10. Hypoxia has been shown to promote the proliferation and differentiation of neural stem cells [55]. Formation of the optic cup largely depends on the size of the optic vesicles [19,23], and the vesicles formed under hypoxia tend to be bigger with a higher probability of optic cup formation. The present results are consistent with those of a study that demonstrated higher efficiency and number of rod photoreceptors cells in two-dimensional (2D) culture under hypoxia conditions [56].

ESCs and iPSCs derived from *Nrl*-GFP mice were used to investigate rod birth and differentiation *in vitro*. As *Nrl* is the earliest rod-specific marker [26], rod photoreceptors in organoid culture are marked by GFP and can be quantified as differentiation proceeds. Thus, we can reliably document the progressive increase in the number of GFP+ cells and GFP intensity in retinal organoid cultures, which include more than 70% GFP+ rods at D35. The GFP+ cells may have been underestimated as intact retinal organoids with some non-retinal tissues were used for quantification. Nevertheless, the data are comparable to 75–80% rods in the mouse retina *in vivo* [50] and consistent with the reported percentage of photoreceptors in retinal organoids from mouse ESCs [23]. Transcriptome analysis of D35 GFP+ cells from retinal organoids revealed their maturation beyond the developing rods in the P6 mouse retina. Efficient differentiation of rods from *Nrl*-GFP ESCs and iPSCs should facilitate their analysis and use in transplantation studies, without additional steps for labeling [21].

With the use of the HIPRO protocol, the organoid cultures were maintained until at least D35. At this stage, the neural retina contained all major cell types, including rod and cone photoreceptors. Limited differentiation of the inner retina neurons from iPSCs derived from fibroblasts has been reported to reflect epigenetic memory [25]; however, the neural retina derived with the HIPRO protocol was stratified, with a substantial number of bipolar and amacrine cells and Müller glia. Consistent with other studies [21,24], retinal ganglion cells are scarce, especially at the late stage of differentiation. As the survival of ganglion cells requires sufficient oxygen and nutrients [57,58], static culture may not be useful for maintaining their long-term survival, and dynamic culture (e.g., using a bioreactor) may be required for retinal organoids.

Another significant observation in the retinal organoids in the present study was the growth of cilia and the initiation of outer segment morphogenesis. As reported previously, proper development of the outer segments requires signaling from the RPE [59]. Previous studies have reported the presence of the RPE in organoid culture but only at an early stage of differentiation [18,19,21]. The RPE appears to be lost as retinal cells proliferate and detach. Coculture or explant culture of the RPE with retinal organoids would be necessary for outer segment biogenesis and phototransduction.

Retinal organoid cultures have wide applications for studies of organ development, disease modeling, and/or treatment design [12,60-64]. With the development of genome editing tools, such as CRISPR/Cas9, a specific cell type can be labeled by fluorescence markers and purified to decipher gene regulatory networks [20,65] or as a source of transplantation [21,23,66]. The present study provides a useful system for efficiently generating retinal organoids with a mature neural retina and provide a framework for developing a more advanced differentiation platform by augmenting nutrients and oxygen supply using bioengineering tools (such as a bioreactor).

## APPENDIX 1.

Differentiation of retinal organoids using the original serum-free floating cultures of embryoid body-like aggregates with quick reaggregation (SFEBq) protocol. No significant morphological differences were observed among neural retinas (NRs) differentiated from ESCs or iPSCs, and the representative figures of NR are shown. Nuclei were stained with 4',6-diamidino-2-phenylindole (DAPI, blue). (A) Morphology of NR. Immunostaining with anti-rhodopsin (Rho, red) antibody marks rod photoreceptors, whereas anti-calbindin (Calb, green) labels both horizontal and amacrine

cells. S-opsin (Opnsw, red) is a marker for S-cones. Amacrine and ganglion cells are labeled by Calretinin (red) and Brn3a (red) immunostaining. Bipolar cells are indicated by Pkcα (red) and Chx10 (red). Scale bar: 100 µm. (B) Relative viability of cells in 30–60 organoids that were counted in each experiment. The survival data from D18 organoids in High Efficiency Hypoxia Induced Generation of Photoreceptors in Retinal Organoids (HIPRO) protocol was set at 100%. Gating by DAPI and forward scatter was used to evaluate cell viability. (C) Percentage of GFP+ cells (rods) in the total cell population from 30 to 60 organoids. No significant differences were observed in the percentage of GFP+ cells from ESCs or iPSCs-derived retinal organoids. The data in (B) and (C) are represented as mean ± SEM and was obtained from 4 independent experiments each from ESC and iPSC organoids (n=4). *$p$<0.05. To access the data, click or select the words "Appendix 1."

## ACKNOWLEDGMENTS

We are grateful to Pinghu Liu, Samantha Papal, Jung-woong Kim, Hiroko Shimada-Ishii, Jacklyn Mahgerefteh, Tyler DiStefano and Jacob Nellissery for insightful discussions and constructive comments. We thank Linn Gieser and Matthew Brooks for assistance with RNA-seq, and Julie Laux, Jessica Albrecht, and Rafael Villasmil for help with flow cytometry. This work was supported by intramural research program of the National Eye Institute (ZIAEY000450, ZIAEY000474).

## REFERENCES

1. Lamb TD. Evolution of phototransduction, vertebrate photoreceptors and retina. Prog Retin Eye Res 2013; 36:52-119. [PMID: 23792002].
2. Wright AF, Chakarova CF, Abd El-Aziz MM, Bhattacharya SS. Photoreceptor degeneration: genetic and mechanistic dissection of a complex trait. Nat Rev Genet 2010; 11:273-84. [PMID: 20212494].
3. Fritsche LG, Fariss RN, Stambolian D, Abecasis GR, Curcio CA, Swaroop A. Age-Related Macular Degeneration: Genetics and Biology Coming Together. Annu Rev Genomics Hum Genet 2014; [PMID: 24773320].
4. Fritsche LG, Igl W, Bailey JN, Grassmann F, Sengupta S, Bragg-Gresham JL, Burdon KP, Hebbring SJ, Wen C, Gorski M, Kim IK, Cho D, Zack D, Souied E, Scholl HP, Bala E, Lee KE, Hunter DJ, Sardell RJ, Mitchell P, Merriam JE, Cipriani V, Hoffman JD, Schick T, Lechanteur YT, Guymer RH, Johnson MP, Jiang Y, Stanton CM, Buitendijk GH, Zhan X, Kwong AM, Boleda A, Brooks M, Gieser L, Ratnapriya R, Branham KE, Foerster JR, Heckenlively JR, Othman MI, Vote BJ, Liang HH, Souzeau E, McAllister IL, Isaacs T, Hall J, Lake S, Mackey DA, Constable IJ, Craig JE, Kitchner TE, Yang Z, Su Z, Luo H, Chen D, Ouyang H, Flagg K, Lin D, Mao G, Ferreyra H, Stark K, von Strachwitz CN, Wolf A, Brandl C, Rudolph G, Olden M, Morrison MA, Morgan DJ, Schu M, Ahn J, Silvestri G, Tsironi EE, Park KH, Farrer LA, Orlin A, Brucker A, Li M, Curcio CA, Mohand-Said S, Sahel JA, Audo I, Benchaboune M, Cree AJ, Rennie CA, Goverdhan SV, Grunin M, Hagbi-Levi S, Campochiaro P, Katsanis N, Holz FG, Blond F, Blanche H, Deleuze JF, Igo RP Jr, Truitt B, Peachey NS, Meuer SM, Myers CE, Moore EL, Klein R, Hauser MA, Postel EA, Courtenay MD, Schwartz SG, Kovach JL, Scott WK, Liew G, Tan AG, Gopinath B, Merriam JC, Smith RT, Khan JC, Shahid H, Moore AT, McGrath JA, Laux R, Brantley MA Jr, Agarwal A, Ersoy L, Caramoy A, Langmann T, Saksens NT, de Jong EK, Hoyng CB, Cain MS, Richardson AJ, Martin TM, Blangero J, Weeks DE, Dhillon B, van Duijn CM, Doheny KF, Romm J, Klaver CC, Hayward C, Gorin MB, Klein ML, Baird PN, den Hollander AI, Fauser S, Yates JR, Allikmets R, Wang JJ, Schaumberg DA, Klein BE, Hagstrom SA, Chowers I, Lotery AJ, Leveillard T, Zhang K, Brilliant MH, Hewitt AW, Swaroop A, Chew EY, Pericak-Vance MA, DeAngelis M, Stambolian D, Haines JL, Iyengar SK, Weber BH, Abecasis GR, Heid IM. A large genome-wide association study of age-related macular degeneration highlights contributions of rare and common variants. Nat Genet 2016; 48:134-43. [PMID: 26691988].
5. Pierce EA, Bennett J. The Status of RPE65 Gene Therapy Trials: Safety and Efficacy. Cold Spring Harb Perspect Med 2015; 5:a017285-[PMID: 25635059].
6. Jacobson SG, Cideciyan AV, Roman AJ, Sumaroka A, Schwartz SB, Heon E, Hauswirth WW. Improvement and decline in vision with gene therapy in childhood blindness. N Engl J Med 2015; 372:1920-6. [PMID: 25936984].
7. Bainbridge JW, Mehat MS, Sundaram V, Robbie SJ, Barker SE, Ripamonti C, Georgiadis A, Mowat FM, Beattie SG, Gardner PJ, Feathers KL, Luong VA, Yzer S, Balaggan K, Viswanathan A, de Ravel TJ, Casteels I, Holder GE, Tyler N, Fitzke FW, Weleber RG, Nardini M, Moore AT, Thompson DA, Petersen-Jones SM, Michaelides M, van den Born LI, Stockman A, Smith AJ, Rubin G, Ali RR. Long-term effect of gene therapy on Leber's congenital amaurosis. N Engl J Med 2015; 372:1887-97. [PMID: 25938638].
8. Dalkara D, Goureau O, Marazova K, Sahel JA. Let There Be Light: Gene and Cell Therapy for Blindness. Hum Gene Ther 2016; 27:134-47. [PMID: 26751519].
9. Chen Y, Palczewski K. Systems Pharmacology Links GPCRs with Retinal Degenerative Disorders. Annu Rev Pharmacol Toxicol 2016; [PMID: 25839098].
10. Adamantidis A, Arber S, Bains JS, Bamberg E, Bonci A, Buzsaki G, Cardin JA, Costa RM, Dan Y, Goda Y, Graybiel AM, Hausser M, Hegemann P, Huguenard JR, Insel TR, Janak PH, Johnston D, Josselyn SA, Koch C, Kreitzer AC, Luscher C, Malenka RC, Miesenbock G, Nagel G, Roska B, Schnitzer MJ, Shenoy KV, Soltesz I, Sternson SM, Tsien RW, Tsien RY, Turrigiano GG, Tye KM, Wilson RI. Optogenetics: 10 years after ChR2 in neurons–views from the community. Nat Neurosci 2015; 18:1202-12. [PMID: 26308981].

11. MacLaren RE, Pearson RA, MacNeil A, Douglas RH, Salt TE, Akimoto M, Swaroop A, Sowden JC, Ali RR. Retinal repair by transplantation of photoreceptor precursors. Nature 2006; 444:203-7. [PMID: 17093405].

12. Jayakody SA, Gonzalez-Cordero A, Ali RR, Pearson RA. Cellular strategies for retinal repair by photoreceptor replacement. Prog Retin Eye Res 2015; 46:31-66. [PMID: 25660226].

13. Homma K, Okamoto S, Mandai M, Gotoh N, Rajasimha HK, Chang YS, Chen S, Li W, Cogliati T, Swaroop A, Takahashi M. Developing rods transplanted into the degenerating retina of crx-knockout mice exhibit neural activity similar to native photoreceptors. Stem Cells 2013; 31:1149-59. [PMID: 23495178].

14. Lamba DA, Gust J, Reh TA. Transplantation of human embryonic stem cell-derived photoreceptors restores some visual function in Crx-deficient mice. Cell Stem Cell 2009; 4:73-9. [PMID: 19128794].

15. Tucker BA, Park IH, Qi SD, Klassen HJ, Jiang C, Yao J, Redenti S, Daley GQ, Young MJ. Transplantation of adult mouse iPS cell-derived photoreceptor precursors restores retinal structure and function in degenerative mice. PLoS One 2011; 6:e18992-[PMID: 21559507].

16. Postel K, Bellmann J, Splith V, Ader M. Analysis of cell surface markers specific for transplantable rod photoreceptors. Mol Vis 2013; 19:2058-67. [PMID: 24146539].

17. Santos-Ferreira T, Postel K, Stutzki H, Kurth T, Zeck G, Ader M. Daylight vision repair by cell transplantation. Stem Cells 2015; 33:79-90. [PMID: 25183393].

18. Eiraku M, Sasai Y. Mouse embryonic stem cell culture for generation of three-dimensional retinal and cortical tissues. Nat Protoc 2012; 7:69-79. [PMID: 22179593].

19. Eiraku M, Takata N, Ishibashi H, Kawada M, Sakakura E, Okuda S, Sekiguchi K, Adachi T, Sasai Y. Self-organizing optic-cup morphogenesis in three-dimensional culture. Nature 2011; 472:51-6. [PMID: 21475194].

20. Kaewkhaw R, Kaya KD, Brooks M, Homma K, Zou J, Chaitankar V, Rao M, Swaroop A. Transcriptome Dynamics of Developing Photoreceptors in Three-Dimensional Retina Cultures Recapitulates Temporal Sequence of Human Cone and Rod Differentiation Revealing Cell Surface Markers and Gene Networks. Stem Cells 2015; 33:3504-18. [PMID: 26235913].

21. Gonzalez-Cordero A, West EL, Pearson RA, Duran Y, Carvalho LS, Chu CJ, Naeem A, Blackford SJ, Georgiadis A, Lakowski J, Hubank M, Smith AJ, Bainbridge JW, Sowden JC, Ali RR. Photoreceptor precursors derived from three-dimensional embryonic stem cell cultures integrate and mature within adult degenerate retina. Nat Biotechnol 2013; 31:741-7. [PMID: 23873086].

22. Assawachananont J, Mandai M, Okamoto S, Yamada C, Eiraku M, Yonemura S, Sasai Y, Takahashi M. Transplantation of embryonic and induced pluripotent stem cell-derived 3D retinal sheets into retinal degenerative mice. Stem Cell Rep 2014; 2:662-74. [PMID: 24936453].

23. Decembrini S, Koch U, Radtke F, Moulin A, Arsenijevic Y. Derivation of traceable and transplantable photoreceptors from mouse embryonic stem cells. Stem Cell Rep 2014; 2:853-65. [PMID: 24936471].

24. Volkner M, Zschatzsch M, Rostovskaya M, Overall RW, Busskamp V, Anastassiadis K, Karl MO. Retinal Organoids from Pluripotent Stem Cells Efficiently Recapitulate Retinogenesis. Stem Cell Rep 2016; 6:525-38. [PMID: 27050948].

25. Hiler D, Chen X, Hazen J, Kupriyanov S, Carroll PA, Qu C, Xu B, Johnson D, Griffiths L, Frase S, Rodriguez AR, Martin G, Zhang J, Jeon J, Fan Y, Finkelstein D, Eisenman RN, Baldwin K, Dyer MA. Quantification of Retinogenesis in 3D Cultures Reveals Epigenetic Memory and Higher Efficiency in iPSCs Derived from Rod Photoreceptors. Cell Stem Cell 2015; 17:101-15. [PMID: 26140606].

26. Akimoto M, Cheng H, Zhu D, Brzezinski JA, Khanna R, Filippova E, Oh EC, Jing Y, Linares JL, Brooks M, Zareparsi S, Mears AJ, Hero A, Glaser T, Swaroop A. Targeting of GFP to newborn rods by Nrl promoter and temporal expression profiling of flow-sorted photoreceptors. Proc Natl Acad Sci USA 2006; 103:3890-5. [PMID: 16505381].

27. Mears AJ, Kondo M, Swain PK, Takada Y, Bush RA, Saunders TL, Sieving PA, Swaroop A. Nrl is required for rod photoreceptor development. Nat Genet 2001; 29:447-52. [PMID: 11694879].

28. Oh EC, Khan N, Novelli E, Khanna H, Strettoi E, Swaroop A. Transformation of cone precursors to functional rod photoreceptors by bZIP transcription factor NRL. Proc Natl Acad Sci USA 2007; 104:1679-84. [PMID: 17242361].

29. Swaroop A, Kim D, Forrest D. Transcriptional regulation of photoreceptor development and homeostasis in the mammalian retina. Nat Rev Neurosci 2010; 11:563-76. [PMID: 20648062].

30. Kim JW, Yang HJ, Oel AP, Brooks MJ, Jia L, Plachetzki DC, Li W, Allison WT, Swaroop A. Recruitment of Rod Photoreceptors from Short-Wavelength-Sensitive Cones during the Evolution of Nocturnal Vision in Mammals. Dev Cell 2016; 37:520-32. [PMID: 27326930].

31. Takahashi K, Yamanaka S. Induction of pluripotent stem cells from mouse embryonic and adult fibroblast cultures by defined factors. Cell 2006; 126:663-76. [PMID: 16904174].

32. Evans MJ, Kaufman MH. Establishment in culture of pluripotential cells from mouse embryos. Nature 1981; 292:154-6. [PMID: 7242681].

33. Ying QL, Wray J, Nichols J, Batlle-Morera L, Doble B, Woodgett J, Cohen P, Smith A. The ground state of embryonic stem cell self-renewal. Nature 2008; 453:519-23. [PMID: 18497825].

34. Bolger AM, Lohse M, Usadel B. Trimmomatic: a flexible trimmer for Illumina sequence data. Bioinformatics 2014; 30:2114-20. [PMID: 24695404].

35. Yates A, Akanni W, Amode MR, Barrell D, Billis K, Carvalho-Silva D, Cummins C, Clapham P, Fitzgerald S, Gil L, Giron CG, Gordon L, Hourlier T, Hunt SE, Janacek SH, Johnson

N, Juettemann T, Keenan S, Lavidas I, Martin FJ, Maurel T, McLaren W, Murphy DN, Nag R, Nuhn M, Parker A, Patricio M, Pignatelli M, Rahtz M, Riat HS, Sheppard D, Taylor K, Thormann A, Vullo A, Wilder SP, Zadissa A, Birney E, Harrow J, Muffato M, Perry E, Ruffier M, Spudich G, Trevanion SJ, Cunningham F, Aken BL, Zerbino DR, Flicek P. Ensembl 2016. Nucleic Acids Res 2016; 44:D1D710-6. [PMID: 26687719].

36. Bray NL, Pimentel H, Melsted P, Pachter L. Near-optimal probabilistic RNA-seq quantification. Nat Biotechnol 2016; 34:525-7. [PMID: 27043002].

37. Soneson C, Love MI, Robinson MD. Differential analyses for RNA-seq: transcript-level estimates improve gene-level inferences. F1000 Res 2015; 4:1521-[PMID: 26925227].

38. Robinson MD, McCarthy DJ, Smyth GK. edgeR: a Bioconductor package for differential expression analysis of digital gene expression data. Bioinformatics 2010; 26:139-40. [PMID: 19910308].

39. Bodenhofer U, Kothmeier A, Hochreiter S. APCluster: an R package for affinity propagation clustering. Bioinformatics 2011; 27:2463-4. [PMID: 21737437].

40. Mitsui K, Tokuzawa Y, Itoh H, Segawa K, Murakami M, Takahashi K, Maruyama M, Maeda M, Yamanaka S. The homeoprotein Nanog is required for maintenance of pluripotency in mouse epiblast and ES cells. Cell 2003; 113:631-42. [PMID: 12787504].

41. Gurdasani D, Carstensen T, Tekola-Ayele F, Pagani L, Tachmazidou I, Hatzikotoulas K, Karthikeyan S, Iles L, Pollard MO, Choudhury A, Ritchie GR, Xue Y, Asimit J, Nsubuga RN, Young EH, Pomilla C, Kivinen K, Rockett K, Kamali A, Doumatey AP, Asiki G, Seeley J, Sisay-Joof F, Jallow M, Tollman S, Mekonnen E, Ekong R, Oljira T, Bradman N, Bojang K, Ramsay M, Adeyemo A, Bekele E, Motala A, Norris SA, Pirie F, Kaleebu P, Kwiatkowski D, Tyler-Smith C, Rotimi C, Zeggini E, Sandhu MS. The African Genome Variation Project shapes medical genetics in Africa. Nature 2015; 517:327-32. [PMID: 25470054].

42. Suda Y, Suzuki M, Ikawa Y, Aizawa S. Mouse embryonic stem cells exhibit indefinite proliferative potential. J Cell Physiol 1987; 133:197-201. [PMID: 3667706].

43. Pistollato F, Chen HL, Schwartz PH, Basso G, Panchision DM. Oxygen tension controls the expansion of human CNS precursors and the generation of astrocytes and oligodendrocytes. Mol Cell Neurosci 2007; 35:424-35. [PMID: 17498968].

44. Chen HL, Pistollato F, Hoeppner DJ, Ni HT, McKay RD, Panchision DM. Oxygen tension regulates survival and fate of mouse central nervous system precursors at multiple levels. Stem Cells 2007; 25:2291-301. [PMID: 17556599].

45. Rodriguez-Boulan E, Macara IG. Organization and execution of the epithelial polarity programme. Nat Rev Mol Cell Biol 2014; 15:225-42. [PMID: 24651541].

46. Liu H, Mohamed O, Dufort D, Wallace VA. Characterization of Wnt signaling components and activation of the Wnt canonical pathway in the murine retina. Dev Dyn 2003; 227:323-34. [PMID: 12815618].

47. Meyer-Franke A, Kaplan MR, Pfrieger FW, Barres BA. Characterization of the signaling interactions that promote the survival and growth of developing retinal ganglion cells in culture. Neuron 1995; 15:805-19. [PMID: 7576630].

48. Gonzalez-Cordero A, West EL, Pearson RA, Duran Y, Carvalho LS, Chu CJ, Naeem A, Blackford SJI, Georgiadis A, Lakowski J, Hubank M, Smith AJ, Bainbridge JWB, Sowden JC, Ali RR. Photoreceptor precursors derived from three-dimensional embryonic stem cell cultures integrate and mature within adult degenerate retina. Nat Biotechnol 2013; 31:741-7. [PMID: 23873086].

49. Zhang X, Serb JM, Greenlee MH. Mouse retinal development: a dark horse model for systems biology research. Bioinform Biol Insights 2011; 5:99-113. [PMID: 21698072].

50. Carter-Dawson LD, LaVail MM. Rods and cones in the mouse retina. II. Autoradiographic analysis of cell generation using tritiated thymidine. J Comp Neurol 1979; 188:263-72. [PMID: 500859].

51. Hao H, Veleri S, Sun B, Kim DS, Keeley PW, Kim JW, Yang HJ, Yadav SP, Manjunath SH, Sood R, Liu P, Reese BE, Swaroop A. Regulation of a novel isoform of Receptor Expression Enhancing Protein REEP6 in rod photoreceptors by bZIP transcription factor NRL. Hum Mol Genet 2014; [PMID: 24691551].

52. Rachel RA, Li T, Swaroop A. Photoreceptor sensory cilia and ciliopathies: focus on CEP290, RPGR and their interacting proteins. Cilia 2012; 1:22-[PMID: 23351659].

53. Wensel TG, Gilliam JC. Three-dimensional architecture of murine rod cilium revealed by cryo-EM. Methods Mol Biol 2015; 1271:267-92. [PMID: 25697530].

54. Lancaster MA, Knoblich JA. Organogenesis in a dish: modeling development and disease using organoid technologies. Science 2014; 345:1247125-[PMID: 25035496].

55. Zhu Z, Shendure J, Church GM. Discovering functional transcription-factor combinations in the human cell cycle. Genome Res 2005; 15:848-55. [PMID: 15930495].

56. Garita-Hernandez M, Diaz-Corrales F, Lukovic D, Gonzalez-Guede I, Diez-Lloret A, Valdes-Sanchez ML, Massalini S, Erceg S, Bhattacharya SS. Hypoxia increases the yield of photoreceptors differentiating from mouse embryonic stem cells and improves the modeling of retinogenesis *in vitro*. Stem Cells 2013; 31:966-78. [PMID: 23362204].

57. Kaur C, Foulds WS, Ling EA. Hypoxia-ischemia and retinal ganglion cell damage. Clin Ophthalmol 2008; 2:879-89. [PMID: 19668442].

58. Tezel G, Yang X, Luo C, Cai J, Kain AD, Powell DW, Kuehn MH, Pierce WM. Hemoglobin expression and regulation in glaucoma: insights into retinal ganglion cell oxygenation. Invest Ophthalmol Vis Sci 2010; 51:907-19. [PMID: 19741249].

59. Nasonkin IO, Merbs SL, Lazo K, Oliver VF, Brooks M, Patel K, Enke RA, Nellissery J, Jamrich M, Le YZ, Bharti K, Fariss RN, Rachel RA, Zack DJ, Rodriguez-Boulan EJ, Swaroop A. Conditional knockdown of DNA methyltransferase 1 reveals

a key role of retinal pigment epithelium integrity in photoreceptor outer segment morphogenesis. Development 2013; 140:1330-41. [PMID: 23406904].

60. Lamba DA, Karl MO, Reh TA. Strategies for retinal repair: cell replacement and regeneration. Prog Brain Res 2009; 175:23-31. [PMID: 19660646].

61. Ader M, Tanaka EM. Modeling human development in 3D culture. Curr Opin Cell Biol 2014; 31:23-8. [PMID: 25033469].

62. Wahlin KJ, Maruotti J, Zack DJ. Modeling retinal dystrophies using patient-derived induced pluripotent stem cells. Adv Exp Med Biol 2014; 801:157-64. [PMID: 24664693].

63. Zhong X, Gutierrez C, Xue T, Hampton C, Vergara MN, Cao LH, Peters A, Park TS, Zambidis ET, Meyer JS, Gamm DM, Yau KW, Canto-Soler MV. Generation of three-dimensional retinal tissue with functional photoreceptors from human iPSCs. Nat Commun 2014; 5:4047-[PMID: 24915161].

64. Kaewkhaw R, Swaroop M, Homma K, Nakamura J, Brooks M, Kaya KD, Chaitankar V, Michael S, Tawa G, Zou J, Rao M, Zheng W, Cogliati T, Swaroop A. Treatment Paradigms for Retinal and Macular Diseases Using 3-D Retina Cultures Derived From Human Reporter Pluripotent Stem Cell Lines. Invest Ophthalmol Vis Sci. 2016;57:ORSFl1-ORSFl1. 27116668

65. Yang HJ, Ratnapriya R, Cogliati T, Kim JW, Swaroop A. Vision from next generation sequencing: multi-dimensional genome-wide analysis for producing gene regulatory networks underlying retinal development, aging and disease. Prog Retin Eye Res 2015; 46:1-30. [PMID: 25668385].

66. Lakowski J, Gonzalez-Cordero A, West EL, Han YT, Welby E, Naeem A, Blackford SJ, Bainbridge JW, Pearson RA, Ali RR, Sowden JC. Transplantation of Photoreceptor Precursors Isolated via a Cell Surface Biomarker Panel From Embryonic Stem Cell-Derived Self-Forming Retina. Stem Cells 2015; 33:2469-82. [PMID: 25982268].

Articles are provided courtesy of Emory University and the Zhongshan Ophthalmic Center, Sun Yat-sen University, P.R. China. The print version of this article was created on 9 September 2016. This reflects all typographical corrections and errata to the article through that date. Details of any changes may be found in the online version of the article.